Residual Bootstrapping on Classified Tensor Morphologies using Constrained Two-Tensor Model

Nagulan Ratnarajah[1]

Andy Simmons[2]

Miguel Bertoni[3]

Ali Hojjatoleslami[1]

[1] Neurosciences and Medical Image Computing, University of Kent, U.K.

[2] Institute of Psychiatry, Kings College London, U.K.

[3] East Kent Hospitals University NHS Foundation Trust, Canterbury, U.K.

Abstract

In this study, a fast and clinically feasible residual-bootstrapping algorithm using a geometrically constrained two-tensor diffusion model is employed for estimating uncertainty in fibre orientation. Voxels are classified based on tensor morphologies before applying a single or two tensor residual-bootstrapping algorithms. Classification of tensor morphologies allows the tensor morphology to be considered when selecting the most appropriate bootstrap procedure. A constrained two-tensor model approach can greatly reduce data acquisition and computational times for whole bootstrap data volume generation compared to other multi-fibre model techniques, facilitating widespread clinical use. Tractography with two-tensor residual-bootstrapping is also developed to estimate the connection probabilities between brain regions, especially regions with complex fibre configurations. Experimental results on a hardware phantom and *in vivo* data demonstrate the superior performance of our approach compared to conventional approaches.

1 Introduction

Bootstrapping of repeated DWMRI data sets allows non-parametric estimation of uncertainty in the inferred fibre orientation [1]. Model-based bootstrap methods (wild-bootstrap [2] and residual-bootstrap [3]) using a single data set have been presented as an alternative to conventional bootstrapping (repetition-bootstrap). Chung et al. [3] demonstrated that the residual-bootstrap performs better than the wild-bootstrap with higher accuracy in estimation of uncertainty. However, model-based and conventional bootstrap tractography methods using DTI can fail when fibre tracts pass through voxels containing complex configurations [4]. These configurations are often characterised by disk-shaped (planar) forms of the tensor. The development of new models based on HARDI seeks to provide solutions to this problem. HARDI-based methods, including multi-tensor models [5] and Q-ball imaging, require longer acquisition times than conventional DTI and are generally not suitable for clinical

applications. To solve some of the above problems, a geometrically constrained two-tensor model for resolving fibre crossings was introduced in [6].

More than a third of voxels in human white matter contain crossing fibre bundles at the current resolution of DWMRI, and these voxels challenge statistical models for tensor estimation and fibre tracking. Therefore, developing a proper bootstrap method for estimating fibre orientation in these voxels is important. Yuan et al. [4] showed that conventional and model-based bootstrapping may fail to quantify the uncertainties in DTI derived parameters in oblate voxels. Therefore, to use bootstrap methods correctly, the morphology of a tensor must be known. The validity of bootstrapping algorithms strongly depends on the correct specification of the fitted model used to estimate tensors. This raises concerns about the validity of bootstrapping those fibre pathways that pass through voxels containing different tensor morphologies. Our solution is to classify tensor morphologies before the application of bootstrap algorithms, which allows the use of appropriate tensor morphologies.

In this work, a residual-bootstrapping algorithm for estimating uncertainty in fibre orientation is presented based on constrained two-tensor diffusion model and voxel tensor morphologies. A probabilistic tractography algorithm is then developed to reconstruct fibre pathways using two-tensor residual bootstrap datasets.

2 Two-Tensor Residual-Bootstrapping Algorithm

Step 1- Data Acquisition and Initial Tensor Fitting. Intensities of the measured diffusion-weighted signals are quantified for a single-tensor model by:

$$S_i = S_0 e^{-b g_i^T D g_i}, \quad i = 1,2,...,N.$$

Applying a log-transformation to the model equation, the estimation of D becomes a well-known multiple linear regression form: $Y_i = (XD)_i + \varepsilon_i, \quad i = 1,2,...,N$, where X is a design matrix of different diffusion gradient directions, $(XD)_i$ is the product of the ith row of X and D, and ε_i is a random sample from the residuals of the original regression model.

To estimate the tensor D, the model-equation is solved by the linear least squares (LLS) method: $\hat{D} = (X^T X)^{-1} X^T Y$. The residuals from the LLS fit used to generate the residual-bootstrap samples in Step 4 are calculated from: $\varepsilon = Y - X\hat{D}$.

Step 2- Classifying Tensor Morphology. To classify tensor morphologies, we developed an algorithm based on three equalities described in Zhu et al. [7], where the algorithm sequentially checks whether each voxel in the image is isotropic, oblate, or prolate. A Two-tensor residual-bootstrap (TTRB) algorithm was applied to oblate voxels and single-tensor residual-bootstrap (STRB) algorithm to the other voxels.

Step 3- Constrained Two-Tensor Model Estimation. A geometrically constrained two-tensor model [6] was used to find the two diffusion tensors and reduce the number of degrees of freedom in the original multi-tensor model [5].This model assumes that both fibre tracts are constrained in the plane spanned by the first two eigenvectors from the single-tensor fit and this now becomes a 2D problem. The gradient vectors are transformed into 2-D coordinate system; $g \rightarrow \tilde{g}$.

$$E(q_i) = S_i/S_0 = f e^{-b\tilde{g}_i^T D_A \tilde{g}_i} + (1-f) e^{-b\tilde{g}_i^T D_B \tilde{g}_i}$$

where D_A and D_B represent the tensor from each compartment, and f and $(1-f)$ are the signal fractions from D_A and D_B. The equation becomes a system of non-linear equations and minimises to $\sum_i (\hat{E}(q_i) - E(q_i))^2$, which gives the estimated tensor elements $\hat{D}_A, \hat{D}_B$ and the fraction $\hat{f}$. The LM optimisation algorithm is used to estimate non-linear equations. In each gradient direction $i (i = 1,...,N)$, a residual ε_i is calculated according to $\varepsilon_i = E(q_i) - \hat{E}(q_i)$.

Step 4- Residual-Bootstrap Sample Generation. The residual vector ε from the single-tensor fit or two-tensor fit used to generate the RB samples. The RB approach assumes that all residuals have similar distributions and a residual value ε_j^* randomly chosen among the set of all residuals ε. Model-based resampling is then performed to construct many data sets, Y^* or $E(q_i)^*$: $Y_j^* = X\hat{D} + \varepsilon_j^*$, for voxels with single-tensor and $E(q_i)_j^* = \hat{E}(q_i) + \varepsilon_j^*$ for voxels with two-tensor. Resampling $\varepsilon^* = [\varepsilon_1^*, \varepsilon_2^*, ..., \varepsilon_N^*]$ and estimating D^* or D_A^* and D_B^* from Y^* or $E(q_i)^*$ are repeated for a fixed large number n to acquire n independent RB samples.
Step 5- Probabilistic Fibre Tractography. Having generated n tensor volumes, a 4^{th} order Runge-Kutta tracking algorithm was used to propagate streamlines bidirectionally from seed points. The algorithm was repeated for n volumes to generate n tracts for each seed point. Every voxel in a volume contains either 1 or 2 principal eigenvectors as appropriate for the tensor morphology of the particular voxel. If the seed point voxel has two tensors then two separate trajectories are generated from the seed point using two fibre orientations. The deterministic tracking algorithm then propagates the trajectories to the next position. If the next position contains two fibre orientations, we choose the diffusion tensor which has the smallest angular difference to the principal eigenvector calculated from the previous position.

3 Methodology

Phantom Data: 3T DW-data were acquired from a physical phantom with 3x3x3 mm^3 voxel resolution, b =1500 s/mm^2 and 64 diffusion directions (www.lnao.fr/spip.php?article106).
***In Vivo* Data:** 3T DTI data were obtained on a healthy volunteer with 2x2x2 mm^3 voxel resolution using 32 diffusion-encoding gradient directions and b = 1300 s/mm^2. The acquisition was repeated 8 times for conventional-bootstrap analysis. The diffusion-weighted images were first corrected for bulk motion and eddy current distortions.
TTRB: We applied the TTRB algorithm to the phantom data and the first of the eight repeated *in vivo* diffusion-weighted datasets and generated 1000 RB volumes. The probabilistic tractography was applied to the RB volumes of phantom data from 4 pre-defined seed positions. Fibre tracts were generated from user-defined regions in *in vivo* data based on prior anatomical knowledge to delineate the corpus callosum (CC), superior longitudinal fasciculus (SLF) and corticospinal tract (CST). A comparison of the results of our method with that of the STRB method applied using the same starting points to extract the same fibre structures in the phantom and *in vivo* data are presented.
TTCB: Two-tensor conventional-bootstrap (TTCB) method was used to randomly generate samples for every voxel in each diffusion-encoded image of the *in vivo* data. In each iteration 5 samples were randomly sampled with replacement from the 8 data acquisitions. The signal for each voxel was calculated as the average of the 5 selected samples. This procedure was repeated for each voxel and diffusion-encoded dataset. The resulting data is one volume bootstrap sample. Single or constrained two-tensor models according to the morphology of the voxels, were fitted to the bootstrap data to estimate diffusion tensors for each voxel. A complete bootstrap tractography dataset was obtained by iteratively running the random sampling method 1000 times to generate multiple volume bootstrap data. Fibre tracts were generated using the same region and the tracking threshold as the TTRB tracking.
Performance Analysis: The phantom data was used to test the performance of the STRB and TTRB probabilistic tracking algorithm. Performance measures were calculated as the error (ξ) in tract estimation, which is a function of distance d from the seed point. The distance d_i at the point (x_i, y_i, z_i), is the cumulative total of all the Euclidian distances of

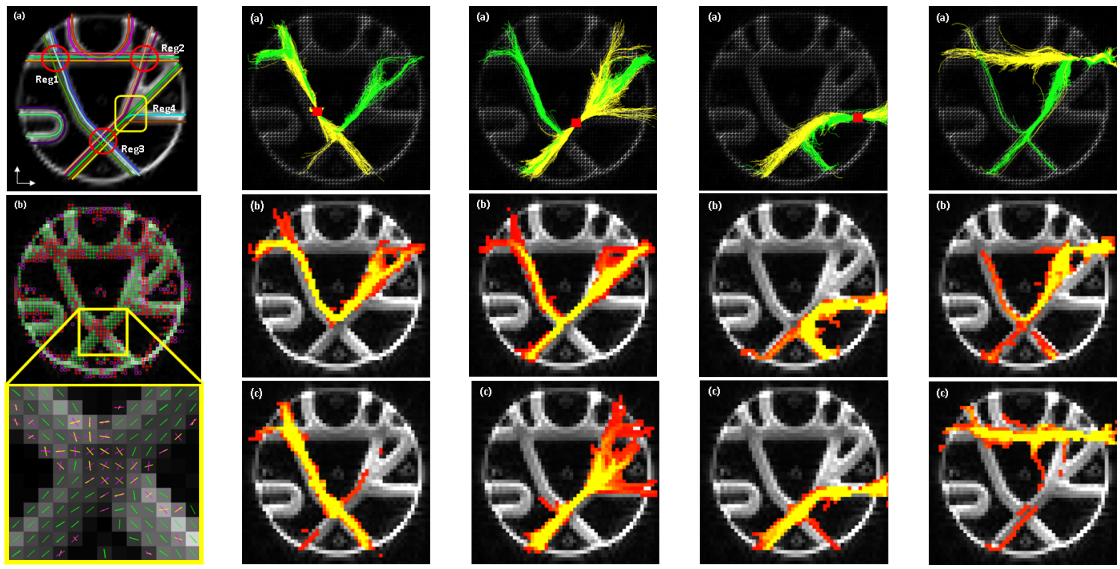

Figure 1: Phantom Data Results (i)(a) Ground truth, crossing regions and a branching region (b) Voxel classification (linear (+), planar(*) or spherical (o) shape) and constrained two-tensor model estimation. (ii)Tracking results from 4 seed points (red square) A, B, C and D. (a) Results of STRB (green) and TTRB (yellow) (b) Probability map of STRB and (c)TTRB.

neighbouring points along the curve up to the point (x_i, y_i, z_i) from the seed point. The positive distances and negative distances are defined by the two directions of a curve from a seed point. The error ξ_i at distance d_i is defined as the Euclidian distance between the ground-truth curve point at d_i and the resultant curve point at d_i from the seed point. The overall range of d is defined as the maximum d at both ends of the ground-truth curve. The ground truth curves and the curves of the two probabilistic methods from the 4 seed points of the phantom data were assessed. From the 1000 probabilistic curves, average error values were computed for each method and for each seed point at 10 mm distances.

4 Results and Discussion

Phantom Data: In Figure 1(A), ideally, one would expect the tractography trajectories starting from the seed point to cross regions 1 and 3; instead as STRB tracts enter the fibre crossing region the fibre tracts diverge in the wrong direction. The TTRB result, however, shows that the trajectories correctly cross the region and tracts are similar to the expected ground truth. In Figure 1(B), the seed point selected as a target shows the branching ability of the TTRB algorithm. The estimated pathways of STRB have leaked and are dispersed, which makes the main pathway of connectivity more difficult to comprehend. For seed points C and D the TTRB tractography correctly follows the fibre direction through the fibre-crossing regions: Region 3 and Region 2, while the STRB results do not.

Performance Analysis: Consider the plots of average error at different distances from the 4 seed points (Figure 2(i)), generally, the error increases with distance from the seed point for both methods. STRB errors largely increase with distance compared with TTRB errors after the tracts enter crossing regions (Region 1, 2, and 3) in all cases, because STRB tracts diverge in the wrong direction (Figure 1 (A), (C) and (D)) in these regions.

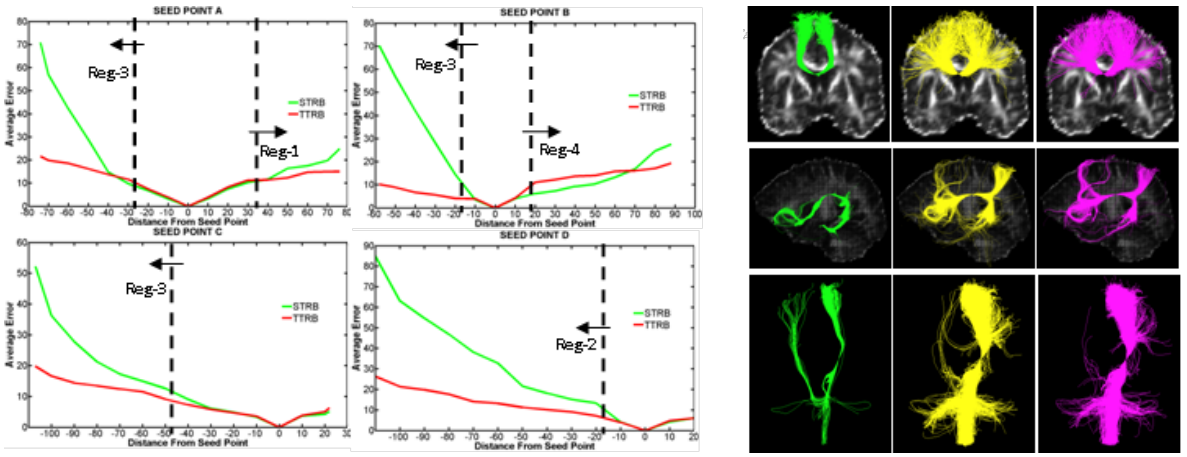

(i) (ii)

Figure 2: (i) Comparison of STRB and TTRB from four seed points A, B,C and D with the average error (in mm) at different distances from the seed point. (ii) *In vivo* tracking results: CC, SLF and CST in rows; STRB,TTRB and TTCB in columns.

***In Vivo* Data:** TTRB fibre tracking techniques were able to more accurately delineate the callosal radiation than STRB tractography (Figure 2 (ii)). The TTRB tractography method was able to traverse regions of crossing fibres and connectivity observed throughout the lateral frontal and parietal lobes while STRB tracts only showed connectivity between the left and right superior frontal gyri of both hemispheres. TTRB tractography results of the SLF show more white matter connections passing through the seed point, demonstrating not only central parts of the SLF, but also fibres reaching more distally, as well as links and projections to parts of the inferior longitudinal fascicle, cingulum and links between subcortical areas, not observed for STRB. The results of the CST illustrate that STRB and TTRB are able to reconstruct the CST from the cortex to the spinal cord from a seed point placed in the internal capsule. STRB results indicate that a number of streamlines erroneously cross and project into the contralateral hemisphere. TTRB and TTCB produced very similar reconstructions of all three tracts and higher fibre dispersion values were observed compared to STRB results, especially as the tracts move further from the seed point.

References

[1] S.Pajevic and P.J.Basser. Parametric and non-parametric statistical analysis of DT-MRI data. *J. Magn. Reson.*, 161:1-14, 2003.

[2] B.Whitcher, D. S.Tuch, and L.Wang. The wild bootstrap to quantify variability in diffusion tensor MRI. in *Proc. ISMRM 13th Annu. Meeting*, 1333, 2005.

[3] S.Chung, Y.Lu, and R.G.Henry. Comparison of bootstrap approaches for estimation of uncertainties of DTI parameters. *NeuroImage*, 33:531-541, 2006.

[4] Y.Yuan, H.T.Zhu, J.G.Ibrahim, B.Peterson, and W.L.Lin. A note on the validity of statistical bootstrapping for estimating the uncertainty of tensor parameters in diffusion tensor images. *IEEE Trans Med Imaging*, 27:1506-1514, 2008.

[5] D.Tuch, T.Reese, M.Wiegell, N.Makris, J.Belliveau, and V.Wedeen. HARDI reveals intravoxel white matter fiber heterogeneity. *Magn. Reson. Med.*, 48(4):577-582, 2002.

[6] S.Peled, O.Friman, F.Jolesz, and C.F.Westin. Geometrically constrained two-tensor model for crossing tracts in DWI. *Magn. Reson. Imaging*, 24:1263-1270, 2006.

[7] H. T.Zhu, D.Xu, R.Amir, X.Hao, H.Zhang, and B.Peterson. A statistical framework for the classification of tensor morphologies in diffusion tensor images. *Magn. Res. Imag.*, 24:569-582, 2006.